Moraines in the Austrian Alps Record Repeated Phases of Glacier Stabilization through the Late Glacial and the Early Holocene

Sandra M. Braumann (sandra.braumann@boku.ac.at)
University of Natural Resources and Life Sciences (BOKU)
Joerg M. Schaefer
Lamont-Doherty Earth Observatory of Columbia University
Stephanie Neuhuber
University of Natural Resources and Life Sciences (BOKU)
Markus Fiebig
University of Natural Resources and Life Sciences (BOKU)

Research Article

Keywords:

Posted Date: February 17th, 2022

DOI: https://doi.org/10.21203/rs.3.rs-1321188/v1

Version of Record: A version of this preprint was published at Scientific Reports on June 12th, 2002. See the published version at https://doi.org/10.1038/s41598-022-12477-x.

Abstract

Climate is currently warming due to anthropogenic impact on the Earth's atmosphere. To better understand the processes and feedbacks within the climate system that underlie this accelerating warming trend, it is useful to examine past periods of abrupt climate change that were driven by natural forcings. Glaciers provide an excellent natural laboratory for reconstructing the climate of the past as they respond sensitively to climate oscillations. Therefore, we study glacier systems and their behavior during the transition from colder to warmer climate episodes, focusing on the period between 15 and 10 ka.

Using a combination of geomorphological mapping and beryllium-10 surface exposure dating, we reconstruct ice extents in two glaciated valleys of the Silvretta Massif in the Austrian Alps and find that the general ice retreat during the deglaciation after the Last Glacial Maximum (LGM) was interrupted by glacier stabilization during the Oldest Dryas to Bølling transition (moraine age: 14.4 ± 1.0 ka), during the Younger Dryas (YD; 12.9-11.7 ka), and during the Early Holocene (EH; 12–10 ka). The first moraine age group indicates a lateral stable ice margin that postdates the 'Gschnitz' stadial (ca. 17–16 ka) and predates the YD. It shows that local inner-alpine glaciers were larger than during the subsequent YD until the onset of the Bølling warm phase (ca. 14.6 ka), or possibly even into the Bølling. The second age group ca. 80 m below the (pre-)Bølling moraine indicates ice extents during the YD cold phase and captures the spatial and temporal fine structure of glacier retreat during this period. The ice surface lowered by 50–60 m through the YD, which is indicative of milder climate conditions at the end of the YD compared to its beginning. Finally, the third age group falls into a period of more substantial warming, the YD–EH transition, and shows discontinuous warming during the glacial to interglacial transition.

The new geochronologies synthesized with pre-existing moraine records from the Silvretta Massif evidence three cold phases that punctuated the general post-LGM warming trend, and illustrate the sensitive response of Silvretta glaciers to abrupt climate oscillations in the past.

1 Introduction

Mountain glaciers are highly sensitive to climate variations, most importantly to changes in summer temperatures and to a lesser extent to changes in precipitation [1,2]. This sensitivity is evident in the accelerating deglaciation of alpine regions caused by rapid warming due to increasing greenhouse gas emissions in recent decades [3, chapter 3, section 3.3]. Deglaciation affects mountain regions in various ways, including altering the hydrological regime in these areas and downstream, impacting ecosystems, and increasing the frequency of natural hazards [4]. Improving our understanding of interactions between the climate system and the cryosphere in the past helps to project the magnitude and impact of environmental change in the future.

Glaciers and their shaping of many parts of the earth's surface in the past [5,6] enable us to explore the climate system and how it operates with and without anthropogenic impact. Detailed geomorphological mapping and direct dating of former ice margins allow us to reconstruct glaciers across time and space and to draw conclusions about the climate conditions that drove glacier advance or retreat in the past. Here, we present ice-margin reconstructions of two glaciated valleys in the Austrian Alps, at Jamtal and Fimbatal, covering the Late Glacial (LG) and the Early Holocene (EH) – a period when the climate was transitioning from a glacial to an interglacial mode.

LG moraines in the European Alps, especially those deposited during the Younger Dryas (YD, ca. 12.9–11.7 ka) termed 'Egesen' moraines, are subject to numerous geochronological studies that provide valuable insights into this last phase of prolonged cooling before Holocene warming [7]. Other periods of climate transition before and after the YD remain more controversial in terms of glacier extents and ice dynamics, for instance, the Bølling-Allerød period (B-A, ca. 14.6–12.9 ka) and the EH (ca. 11.7–9 ka). Although glaciers were presumably much more extensive at the beginning of the B-A compared to the beginning of the EH, they were driven by a similar climatic pattern during both periods: a steep temperature increase which led to rapid deglaciation. For the period between ca. 12 and 10 ka, moraine chronologies from different places in the Alps, including data presented in this study, have shown that ice retreat and therefore warming was not linear, but was interrupted by centennial-scale cooling [8–11]. For the (pre-)Bølling period, it is still unclear whether ice retreat was steady and of such magnitude that most glaciers in the European Alps retreated to the highest cirques or disappeared altogether [7]. The objective of this study is to contribute to these less resolved periods and to view climate transitions from glacial to interglacial conditions through the lens of glacial geomorphology. Therefore, we mapped moraine sequences at two alpine valleys, the Jamtal and the Fimbatal, and applied ^{10}Be surface exposure dating to selected landforms to produce direct spatial and temporal information of former ice extents in the Silvretta Massif.

The Silvretta Massif is in the westernmost part of the Eastern European Alps (Figure 1a). The mountain range belongs to the Upper Eastern Alpine ("Oberostalpin") tectonic unit and consists of crystalline rocks that have undergone several metamorphic events since their formation during the Precambrian [12]. Lithologies in the valleys include amphibolites, different types of metasediments, and gneisses [13]. Glaciers in the region are temperate and are sensitive to climate oscillations (Figure 2). Over the past 150 years, rapidly increasing greenhouse gas emissions and resulting warming have led to the melting of glacial ice across the planet. In the Silvretta region, the ice-covered area has decreased to 32 ± 2 % of the extent of the Little Ice Age (LIA; ca. 1250–1850 CE) in the reference years 2017/2018 (Figure 1b) [14]. Jamtal glacier – the main ice body at Jamtal – has retreated to a position ca. 2 km upstream from the LIA maximum. In 2018, it covered approximately 2.8 km² with its terminus at an altitude of ca. 2410 m a.s.l. Glaciers at Fimbatal have largely disappeared today with only a few small patches of dead ice left in the uppermost sections of the valley (Figure 1b). In deglaciated sections of both valleys, sequences of lateral and terminal moraines are preserved that evidence stable ice margins of the past and promise insights into periods when climate conditions were favorable for larger glaciers (Figures 3-5, **Figure S2**).

2 Results

A total of 15 rock samples were collected from moraines at Jamtal (n=9) and Fimbatal (n=6). Ages are stratigraphically in order and are presented from old to young, beginning with the Jamtal (JAM) record, followed by the Fimbatal (FMB) record. ^{10}Be analytical data and boulder ages are presented in Table 1 and in Figures 3-5 as well as in the supplement (**Tables S1 and S2, section S4**).

Table 1

^{10}Be analytical data and corresponding exposure ages of Jamtal samples. Samples were analyzed at the CAMS-LLNL. All samples were measured against t
10^{-12} [82]. One to two procedural blanks were processed with each batch of samples with ratios ranging from 2.3 to 8.4 x 10^{-16} (Table S2). The ^{10}Be backgrou
subtracted from the samples. Exposure ages were calculated with the calculator formerly known as CRONUS-Earth online calculator v3; [83], using the Swiss ^{10}
scheme. Ages are calculated relative to the sampling year denoted by the first number in the sample ID and are rounded to the nearest 10 years. Uncertainties c
1% uncertainty on the carrier concentration.

	Sample ID	Latitude [DD]	Longitude [DD]	Elevation [m a.s.l.]	Av. thickness [cm]	Shielding factor	Quartz mass [g]	^{9}Be carrier [g]	^{10}Be/^{9}Be ratio ±1σ analytical unc. (10^{-14})				^{10}Be atoms ±1σ analytical unc. [atoms]		
F5b	**FMB-18-05**	46.9436	10.2698	2040	2.1	0.9677	4.5939	0.1821	10.26	±	0.20	(2.0%)	1283934	±	252
	FMB-19-12	46.9435	10.2699	2041	1.7	0.9702	10.6165	0.1789	19.79	±	0.37	(1.9%)	2440545	±	455
F5a	**FMB-18-04**	46.9429	10.2697	2044	1.8	0.9709	42.9287	0.1789	79.07	±	1.68	(2.1%)	9716105	±	205
	FMB-18-08	46.9438	10.2688	2043	2.0	0.9675	25.5955	0.1787	48.96	±	0.91	(1.9%)	6008892	±	111
	FMB-18-09	46.9438	10.2689	2042	2.1	0.9703	23.8501	0.1790	34.29	±	0.64	(1.9%)	4215324	±	792
	FMB-19-13	46.9432	10.2694	2044	1.6	0.9728	10.5569	0.1758	18.60	±	0.35	(1.9%)	2254712	±	421
J7	**JAM-18-11**	46.8904	10.1871	2520	1.3	0.9634	9.2555	0.1806	30.46	±	0.56	(1.9%)	3778652	±	700
	JAM-19-19	46.8904	10.1875	2522	2.0	0.9607	10.6142	0.1798	34.00	±	0.64	(1.9%)	4214518	±	788
	JAM-20-23	46.8904	10.1872	2521	2.9	0.9620	11.3598	0.1807	35.08	±	0.71	(2.0%)	4383259	±	887
J6	**JAM-18-13**	46.8901	10.1838	2432	3.4	0.9781	16.5606	0.1806	44.59	±	0.83	(1.9%)	5532868	±	103
	JAM-19-20	46.8893	10.1865	2445	1.5	0.9604	10.6338	0.1801	26.96	±	0.50	(1.9%)	3347499	±	626
J5	**JAM-20-24**	46.8895	10.1829	2380	2.4	0.9779	6.8428	0.1805	15.93	±	0.30	(1.9%)	1987961	±	370
	JAM-20-25	46.8893	10.1835	2389	1.7	0.9768	10.9885	0.1798	26.46	±	0.52	(2.0%)	3289758	±	648
J3-4	**JAM-20-26**	46.8898	10.1740	2065	1.8	0.9412	11.5032	0.1796	18.81	±	0.40	(2.1%)	2335435	±	498
	JAM-20-27	46.8908	10.1733	2047	1.4	0.9499	11.5197	0.1803	20.97	±	0.39	(1.9%)	2613912	±	485

At **Jamtal**, our focus was on a steep (>30°) valley flank that features a right-lateral moraine set which was shaped by a former tributary glacier (Futschöl glacier; Figures 3a-b, S2, and S3). The uppermost landform selected for ^{10}Be surface exposure dating is **J7** at an elevation of ca. 2520 m a.s.l. (Figure 4a). The three sampled boulders rest on a till-covered lineament and yield a landform age of **14.4 ± 1.0 ka (Figure S1a)**. Around 80 m lower, at ca. 2440 m a.s.l., a sharp-crested moraine (**J6**) was deposited that consists mainly of fine sediments (Figure 4b) and features two boulders that qualified for sampling. Corresponding ages are 12.9 ± 0.2 ka and 12.1 ± 0.2 ka. The ice margin geomorphology another level below denoted as **J5** (Figure 4d), differs from J6 in the absence of a distinct ridge and in the abundance of boulders of which two were selected for dating and yield ages of 11.6 ± 0.2 ka and 11.8 ± 0.2 ka. Two boulders in the main valley embedded in lateral and in terminal moraines (**J3–4**, Figure 3c-d) give ages of 10.4 ± 0.2 ka and 11.6 ± 0.2 ka and extend the Holocene moraine chronology published for the valley by Braumann, et al. [9].

At **Fimbatal**, samples were collected from two adjacent latero-frontal moraine ridges (**F5a** and **F5b**) deposited at an elevation of ca. 2040 m a.s.l. (Figure 5). The outer ridge (**F5b**) consists of mostly fine sediments and is overgrown by vegetation. It is preserved only on the east side of the creek and has few boulders exposed, two of which were sampled and yield ages of 14.0 ± 0.3 ka (FMB-18-05) and 11.6 ± 0.2 ka (FMB-19-12). Although FMB-18-05 agrees within errors with boulder ages along J7 at Jamtal, we reject the age as an outlier due to its stratigraphic position. A terminal moraine at Fimbatal, which is equivalent to the lateral ice-margin position at Jamtal, should be positioned further downstream. FMB-18-05 probably overestimates the age of F5b, most likely due to inheritance from one or multiple earlier exposure events.

The inner ridge (**F5a**) is preserved on both sides of the creek and exhibits a blocky structure in its frontal section caused by the outwash of fine-grained material. Exposure ages of the four boulders along F5a range between 11.9 ± 0.2 ka and 9.1 ± 0.2 ka. The age of FMB-18-09 (9.1 ± 0.2 ka) falls within a period during the Holocene when most glaciers had probably retreated inboard the subsequent LIA ice margin [15–17]. For reference, the LIA terminal moraine in this valley is located at an elevation of ca. 2520 m a.sl., i.e. around 500 m higher and almost 7 km upstream of F5a/b (Figure 1b). These vertical and lateral distances cannot be reconciled with the age and location of FMB-18-09. Therefore, we discard the age for our interpretation. Ages of the remaining moraine boulders featured by F5a in concert with the age of FMB-19-12 of F5b correlate with the moraine age of J5 at Jamtal. The Fimbatal geochronology hence makes a case for two closely spaced stable ice margins toward the end of the YD.

3 Discussion

Boulder ages in both valleys fall into three periods: **(1)** the Oldest Dryas to Bølling (J7), **(2)** the Younger Dryas (J6, J5, F5a, and F5b), and **(3)** the early Holocene (J3–4), and are discussed in this order.

Pre-Bølling to Bølling transition

The deposition of J7 (14.4 ± 1.0 ka) occurred during a period when regional climate was transitioning from stadial to interstadial conditions, i.e., from the Oldest Dryas cold phase to the Bølling warm phase. We review deglaciation of the European Alps in the millennia before the deposition of J7 to place the new moraine records at Jamtal and Fimbatal in a coherent temporal and spatial context of the Alpine LG.

During the Gschnitz stadial, a well-documented post-LGM glacier readvance around 17–16 ka, the uppermost sections of the Alpine main valleys and their tributary valleys were glaciated [18]. This phase of readvance that is often associated with Heinrich event 1 in the North Atlantic [19] was followed by a period of still relatively low mean annual temperatures, but slightly increasing summer temperatures paralleling increasing solar insolation (Figures 6a and 6e). Despite the probably cold winters, glaciers in the Alps responded to the warmer summers after 16 ka [20] and retreated to higher elevations. Several recent studies have investigated the pace of post-LGM deglaciation in selected inner-alpine pass regions by applying surface exposure dating to bedrock sections along transects [21–27]. Results indicate that major ice transfluence zones, for instance, the Gotthard, the Grimsel, and the Simplon passes became ice-free between ca. 16 and 14 ka. However, local glaciers with extents that exceeded the subsequent YD glaciation may have been present until the Bølling. At Jamtal, the deposition of a moraine outboard the Egesen moraines around 14.4 ± 1.0 ka confirms the timing of ice decay reconstructed in these deglaciation studies and indicates that glacier retreat between ca. 16 ka and ca. 14 ka was discontinuous.

Since LG moraines provide geomorphological evidence of discontinuous deglaciation, their identification in alpine valleys allows inferences about cold phases that interrupted the general post-LGM warming trend. The relative moraine stratigraphy of the Alpine region is based on this approach and suggests up to six more or less recognized stadials [28,29], most prominently the above described ‘Gschnitz’ stadial, and the subsequent, upstream ‘Egesen’ stadial. Egesen moraines are distinct multi-ridge structures ubiquitous in high-Alpine valleys and are accepted as the morphostratigraphical equivalent of YD cooling [7,30,31]. A less conspicuous stadial, proposed as a stable ice margin in between the Gschnitz and the Egesen moraines, is the putative ‘Daun’ stadial. Daun moraines are described as recessional moraines, with less pronounced crests, often with few boulders, and sometimes affected by solifluction. They are assumed to indicate pre-Bølling glaciers that are limited to local, inner-alpine locations, being closer to the subsequent Egesen moraines than to Gschnitz. The presence of corresponding moraines in the Alps is sparse, therefore its acknowledgment as an independent stadial that is discernable at several sites across the Alps remains controversial [32]. The underrepresentation of presumable Daun moraines in geochronological studies in the Alps may be owed to their unspectacular morphology in tandem with poorer preservation, and fewer datable boulders. Nevertheless, the morphology and age of several landforms in the Alps, including the J7 moraine at Jamtal, resemble the characteristics of the Daun stadial. In a geochronological study at the Great Aletsch glacier, Schindelwig, et al. [10] investigated an ice margin indicative of glacier extents that exceed the Egesen extent. They obtained a (recalculated) age of 14.4 ± 0.7 ka (their sample VBA-7) for a boulder sitting on top of a bedrock section that deglaciated at the same time. The authors interpret the site as an LG ice margin of the Great Aletsch glacier. Böhlert, et al. [26] yielded a (recalculated) age of 15.2 ± 1.9 ka for a boulder (their sample VM7) embedded in a lateral moraine outboard the presumable Egesen moraine at Val Mulix (Switzerland) and ascribed the landform to the Daun stadial. Rolland, et al. [27] combined the analysis of proglacial lake sediments in the Argentera-Mercantour Massif with exposure dating of glacial features in the region and identified an LG moraine that was deposited ca. 14.6 ± 0.9 ka (Vens moraine, n = 3). These dated boulders and landforms, albeit limited in number, are in good agreement with the age of J7 and suggest moraine formation between ca. 16 and 14 ka in the Alps. However, any attempt to correlate J7 with the traditional Daun stadial first requires the geomorphological evaluation and dating of the type locality in the Austrian Stubai Alps [33].

Considering the age range of J7 (14.4 ±1.0), the landform could also have been deposited at the onset of the Bølling interstadial, during the Older Dryas cold snap (ca. 14 ka), or even during the subsequent Allerød interstadial (until 12.9 ka). The B-A interstadial was identified in numerous climate archives in the Northern Hemisphere [34–38]. Its onset around 14.6 ka is characterized by an abrupt temperature increase that induced substantial changes in environmental and vegetational conditions [39,40]. Summer temperatures increased by several degrees in the Alps [35,37], transitioning from cooler stadial to warmer interstadial levels (Figure 6c-d). Glaciers responded to this warming and might have retreated to the highest cirques of the Alps or disappeared completely during the B-A temperature plateau. The demise of glaciers during this interstadial appears in conflict with concurrent moraine formation of the J7 moraine outboard the subsequent Egesen ice margin. Yet, weakening of the Atlantic Meridional Overturning Circulation (AMOC) may explain centennial-scale cooling during general warming and contemporaneous stabilization or readvance of glaciers in the European Alps. Freshwater input into the North Atlantic Ocean during the deglaciation of adjacent ice sheets has the potential to decelerate or even shut down the warm northwards flowing AMOC limb and to temporarily reduce heat transport to Northern Europe [41,42]. Evidence of repeated freshening of ocean water between 15.8 and 12.6 ka has for instance been detected in a sediment core south of Iceland and has been linked to the deglaciation of the Laurentide ice sheet [43]. A reduction of poleward heat transport may have led to centennial-scale episodes of cooling detected in Northern and Central Europe, such as the Older Dryas and the later Gerzensee oscillations (13.3-13.0 ka) [39]. The link between the deglaciation of the Laurentide ice sheet, resulting in freshwater input into the North Atlantic, and cooling in Europe has been suggested as an explanation for abrupt centennial-scale cooling in the context of the YD-Holocene transition [44,45]. Moraine formation as a result of this teleconnection during the YD-Holocene transition has recently been proposed by Young, et al. [46] for the Greenland ice sheet, by Protin, et al. [8] for mountain glaciers in the French Alps, and by Braumann, et al. [9] for the Austrian Alps. Comparing the warming during the pre-Bølling to Bølling transition and during the YD-Holocene transition (Figure 6e), we tentatively suggest brief episodes of an AMOC weakening and subsequent cooling in Europe. Even though the causation between Bølling warming, freshwater input into the Atlantic, and the AMOC circulation is elusive, we note that the timing of Bølling warming parallels MWP1A, a sea-level rise of about 12–22 m within a few centuries (Figure 6b) [47]. The source of MWP1A remains under debate and has often been attributed to the Antarctic ice sheet alone [48]. However, recent sea-level fingerprinting and ice sheet modeling studies suggest that the melting of ice sheets in the Northern Hemisphere likely has contributed to massive sea-level rise at that time and may have caused centennial-scale cold lapses [49–51].

Both scenarios – moraine deposition prior to or during the Bølling – are plausible, but more direct age data covering that period are needed to better constrain moraine deposition and thus cooling between 16–14 ka in the European Alps. Interestingly, when comparing the (pre-)Bølling moraine age of J7 with mountain glacier records beyond the Alps, we find similar intervals of moraine formation in Norway [52,53], in Patagonia [54–58] and New Zealand [59,60], and the Himalaya region [61]. In the Southern Hemisphere, the climatic explanation for this phase of glacier advance is the Antarctic Cold Reversal (ACR; 14.5-12.7 ka), a millennial-scale cold phase documented in Antarctic ice cores [62]. The extent to which this cold phase propagated from Antarctica and the Southern Hemisphere further to the North remains controversial but we note that moraine formation indicated by J7 falls within the early phase of the ACR.

Younger Dryas – Egesen moraines

The next LG time slice that is captured by the new moraine chronologies of both valleys is the YD period. We interpret moraines J6 and J5 at Jamtal and F5a and F5b at Fimbatal as Egesen moraines that portray the fine structure of ice retreat during this final stadial before Holocene warming (Figure 6e). J6 at Jamtal indicates an ice margin in the early phase of the YD. The lower J5 moraine and F5a/b at Fimbatal delimit glacier extents toward the very end of the YD. Exposure ages from these landforms confirm relative age estimates from a previous study in the Silvretta region that focused on geomorphology and stratigraphy [63].

The Egesen moraine sequence at Jamtal shows that the ice surface lowered by about 55 m from J6 (ca. 2440 m a.s.l.) to J5 (2385 m a.sl.) within a few centuries (Figure 4c), hence supporting the hypothesis that climate conditions became gradually milder through the YD [64]. Glacier retreat with intermittent phases of glacier stabilization through the YD is observed at different places of the Northern Hemisphere [7,52,65] and coincides with slightly increasing summer temperatures (Figure 6e) [34,35,66]. The mountain glacier record of the Southern Hemisphere indicates moraine deposition through glacier retreat during the same time interval [57,67], which corroborates the gradual expansion of YD cooling towards the Southern Hemisphere [68].

Early Holocene

Ice-surface lowering during the YD from J6 to J5 was rapid but the rate of glacier change during the transition from the YD to the EH was even faster. The downwasting of Jamtal glacier and its tributary Futschöl glacier during this period is best illustrated by comparing moraine segments J5 and to J3–4 (Figure 3). Even though the boulder ages of J5 and JAM-20-27 (J3–4) are statistically indistinguishable, the associated landforms indicate very different glacier positions (**Figure 7a-b**). J5 marks the right-lateral ice margin of the tributary (Futschöl) glacier when it still converged with the main (Jamtal) glacier. In turn, J3–4 indicates much smaller glacier extents when the main and the tributary glaciers were separated, which implies deglaciation of the valley flank within a few centuries (Figure 3a, S2). The new early Holocene terminus of Jamtal glacier marked by JAM-20-27 (Figure 3d) is located only around 900 m outboard the Holocene/LIA moraine (**Figure 7c**). J3–4 is interpreted as the equivalent of the right lateral early Holocene moraine set (JR3–4) that was mapped and dated in a previous study [9], which in concert with the adjacent EH Laraintal chronology indicates moraine deposition and thus glacier stabilization ca. 11.0 ± 0.7 ka (Figures 6f, 7b, and S1). The timing of moraine formation overlaps with the Preboreal Oscillation, a centennial-scale cold pulse in (Northern) Europe which was likely caused by AMOC weakening due to freshwater input into the Atlantic – the same mechanism that was tentatively proposed earlier for the deposition of J7 during the early Bølling (**section 3.1**). Similar to the (pre-)Bølling and YD period, the synchronicity of mountain glacier stabilization during the EH is observed in glaciated regions of both hemispheres [46,69–72].

Silvretta glaciers probably remained outboard their subsequent LIA ice margins for the next several centuries but retreated to LIA-like configurations around 10 ka, which is shown based on a ^{10}Be moraine chronology from the adjacent Ochsental (**Figure 7c**) [17]. Throughout the rest of the Holocene, they oscillated inboard the 10 ka limits (e.g., **Figure 7d**) with advances(s) to this position possibly during the Neoglacial and certainly during the LIA [73].

Broader relevance of the new moraine chronologies

The ^{10}Be datasets from the Silvretta Massif are to date the most detailed cosmogenic-nuclide-based mountain glacier records in the Eastern European Alps. They pinpoint the timing of moraine formation in the region around 14.4 ± 1.0 ka, during the YD between 12.9 and 11.7 ka, and during the Early Holocene around 11.0 ± 0.7 ka [9] and around 9.9 ± 0.7 ka [17]. They allow for robust glacier reconstructions at different times during the LG and the Holocene, contribute to our understanding of the climate transitioning from glacial to interglacial conditions, and provide valuable constraints for the modeling of paleoglaciers.

A comparison of the mountain glacier record on a global scale shows that glaciers in both hemispheres deposited moraines around 15–14 ka, during the YD, and during the EH. The next step is to investigate whether these similarities are coincidental, or due to large-scale climatic forcing.

The reconstruction of Silvretta glaciers during recent geological periods shows their sensitive response to natural warming and places the magnitude and impact of anthropogenic climate change in a natural context.

Methods

Geomorphological mapping

Hertl [63], and references therein developed a relative moraine stratigraphy for the region on which this work is based. The pre-existing geomorphological maps were updated and supplemented with information gained during several field campaigns in the summers of 2018 to 2021, from remote sensing data [74,75] and drone imagery. Glacier reconstructions of Jamtal glacier for the Holocene including corresponding maps are presented in Braumann, et al. [9]. With this study, we extend the Jamtal glacier chronology into the LG and focus on landforms that evidence glacier oscillations during that period by mapping and dating margins outboard the Holocene moraines. Reconstructions of paleoglaciers are complemented with glaciological data of modern, annual- to decadal-scale glaciological data including observations of glacier mass balances, front variation, and ice-covered area [14,76–78].

Surface exposure dating with ^{10}Be

When fresh quartz-containing rock surfaces are exposed to cosmic radiation, the production of the cosmogenic radionuclide ^{10}Be begins according to the nuclide-specific production rate (ca. 4 atoms $^{-g}$ $^{-yr}$). The longer a surface has been exposed, the more ^{10}Be accumulates [79]. Thus, the nuclide content in rock surfaces is a function of exposure time. This principle is used in the application of surface exposure dating to glacial landforms. A moraine boulder that is sampled for ^{10}Be analysis has ideally been eroded from bedrock beneath the glacier, has then been transported sub- or englacially, and has finally been deposited on a moraine crest that marks a stable ice margin. It has therefore not been exposed to cosmic radiation before its deposition on the moraine so that its radionuclide inventory is 'zeroed'. If these assumptions are true, the ^{10}Be inventory measured in a rock surface after exposure will produce an age that reflects the boulder's melt out of glacial ice, or in other words, the onset of ice retreat, hence warming.

Rock samples were collected using an electric saw and hammer and chisel. The sample location was measured using a hand-held GPS device. Strike and dip angles of sampled rock surfaces were quantified using a geological compass. Samples were preferably collected from boulder tops at windswept locations to minimize shielding effects due to snow and/or sediment cover. We avoided surfaces that were affected by exfoliation and prioritized boulder locations with striations preserved on the surface, which is indicative of low postglacial erosion. For more details on our sample selection criteria, we refer to Braumann, et al. [17]'s supplement, their Table S1.

Mechanical sample preparation was accomplished at the Department of Lithospheric Research of the University of Vienna and at the Lamont-Doherty Earth Observatory (LDEO). Whole-rock samples were crushed to grain sizes between 63 and 500 µg using a mill or a jaw crusher. Mineral separation strategies included magnetic separation, boiling with phosphoric acid, froth flotation, density separation and repeated (>3) leaches with hydrofluoric acid and nitric acid at concentrations between 1% and 5% [80]. Purified quartz yields, the target mineral for ^{10}Be extraction, ranged from 1.1–11.3% (**Table S1**). Samples were processed in four batches (**Table S2**) with quartz weights ranging from 4.5939 g to 42.9287 g (Table 1). All samples were spiked with the LDEO ^{9}Be carrier (#7) made of deep-mine beryl which has a concentration of approximately 1000 ppm. The extraction of ^{10}Be was accomplished following the LDEO protocol described in LDEO [81]. Isotope ratios in samples (^{10}Be/^{9}Be) were measured at the Center for Accelerator Mass Spectrometry (CAMS) facility, Lawrence Livermore National Laboratory (LLNL) using the 07KNDSTD3110 standard with a ^{10}Be/^{9}Be ratio of 2.85×10^{-12} [82].

Exposure age calculations including statistical outlier identification (X^2 test) were performed using the online calculator formerly known as the CRONUS-Earth online calculator v3 [83]. We used the local 'Swiss' production rate [84] and chose the time-dependent 'Lm' scaling scheme [85]. In the data presentation and discussion, we distinguish between exposure ages of individual boulders and moraine ages. Boulder ages are reported with 1σ analytical uncertainties and a 1 % error on the carrier concentration, but without uncertainties on the production rate as this source of uncertainty is constant for all boulders sampled from the same area. For moraine ages ($n \geq 3$), the production rate error is propagated in quadrature to analytical and carrier uncertainties to allow the correlation of robust landform ages with moraine records from other regions.

Declarations

Acknowledgements

This study was sponsored by inatura Museum GmbH and is based upon work supported by the National Science Foundation under grant no. NSF-1853881. SMB is a recipient of a DOC Fellowship of the Austrian Academy of Sciences (OeAW) at the Institute of Applied Geology, University of Natural Resources and Life Sciences (BOKU) Vienna. For research visits at the Lamont-Doherty Earth Observatory (LDEO) of Columbia University, SMB received a Marietta Blau scholarship sponsored by OeAD GmbH, a Marshall Plan scholarship provided by the Austrian Marshall Plan Foundation and financial support from BOKU's 'Transitions to Sustainability' (T2S) doctoral school. SMB thanks the LDEO cosmogenic nuclide laboratory staff Roseanne Schwartz and Jean Hanley for advice during sample processing and Alan J. Hidy at CAMS-LLNL for ^{10}Be sample analysis. SMB is grateful to Dominik Blasenbauer for assistance in the field, and to Allie Balter-Kennedy for helpful discussions on the topic of this manuscript.

Author Contribution

SMB and JMS designed the study. All authors carried out field work. SMB accomplished cosmogenic nuclide sample preparation and age calculation. SMB wrote the manuscript and prepared the figures. All authors made substantial contributions to the data interpretation and revised and edited the manuscript.

Data availability

All analytical information associated with cosmogenic nuclide measurements is listed in the tables in the Supplement and will be made available via the ICE-D Alpine database (http://alpine.ice-d.org/).

References

1 Huston, A., Siler, N., Roe, G. H., Pettit, E. & Steiger, N. J. Understanding drivers of glacier-length variability over the last millennium. The Cryosphere **15**, 1645-1662, doi:10.5194/tc-15-1645-2021 (2021).

2 Oerlemans, J. Extracting a climate signal from 169 glacier records. Science **308**, 675-677 (2005).

3 IPCC. Climate Change 2021: The Physical Science Basis. Contribution of Working Group I to the Sixth Assessment Report of the Intergovernmental Panel on Climate Change. (2021).

4 Hock, R. et al. in IPCC Special Report on the Ocean and Cryosphere in a Changing Climate (eds H.-O. Pörtner et al.) 131-202 (IPCC - Intergovernmental Panel on Climate Change, 2019).

5 Salcher, B., Prasicek, G., Baumann, S. & Kober, F. Alpine relief limited by glacial occupation time. Geology **49**, 1209-1213, doi:10.1130/G48639.1 (2021).

6 Cunningham, M. T., Stark, C. P., Kaplan, M. R. & Schaefer, J. M. Glacial limitation of tropical mountain height. Earth Surf Dynam **7**, 147-169, doi:10.5194/esurf-7-147-2019 (2019).

7 Ivy-Ochs, S. Glacier Variations in the European Alps at the End of the Last Glaciation. Cuad Investig Geogr **41**, 295-315, doi:10.18172/cig.2750 (2015).

8 Protin, M. et al. Millennial-scale deglaciation across the European Alps at the transition between the Younger Dryas and the Early Holocene – evidence from a new cosmogenic nuclide chronology. Boreas **50**, 671–685, doi:10.1111/bor.12519 (2021).

9 Braumann, S. M. et al. Early Holocene cold snaps and their expression in the moraine record of the eastern European Alps. Clim. Past **17**, 2451-2479, doi:10.5194/cp-17-2451-2021 (2021).

10 Schindelwig, I., Akcar, N., Kubik, P. W. & Schlüchter, C. Lateglacial and early Holocene dynamics of adjacent valley glaciers in the Western Swiss Alps. J Quaternary Sci **27**, 114-124, doi:10.1002/jqs.1523 (2012).

11 Schimmelpfennig, I. et al. Holocene glacier culminations in the Western Alps and their hemispheric relevance. Geology **40**, 891-894, doi:10.1130/G33169.1 (2012).

12 Friebe, G. Geologie der österreichischen Bundesländer - Vorarlberg. 174 (Verlag der Geologischen Bundesanstalt, 2007).

13 Fuchs, G. & Oberhauser, R. 170 Galtür. (1990).

14 Fischer, A., Schwaizer, G., Seiser, B., Helfricht, K. & Stocker-Waldhuber, M. High-resolution inventory to capture glacier disintegration in the Austrian Silvretta. Cryosphere **15**, 4637-4654 (2021).

15 Nicolussi, K. & Patzelt, G. Discovery of early-Holocene wood and peat on the forefield of the Pasterze Glacier, Eastern Alps, Austria. Holocene **10**, 191-199, doi:10.1191/095968300666855842 (2000).

16 Patzelt, G. Das Bunte Moor in der Oberfernau (Stubaier Alpen, Tirol) – Eine neu bearbeitete Schlüsselstelle für die Kenntnis der nacheiszeitlichen Gletscherschwankungen der Ostalpen. Jahrbuch der Geologischen Bundesanstalt **Band 156**, 97-107 (2016).

17 Braumann, S. M. et al. Holocene glacier change in the Silvretta Massif (Austrian Alps) constrained by a new Be-10 chronology, historical records and modern observations. Quaternary Sci Rev **245**, doi:10.1016/j.quascirev.2020.106493 (2020).

18 Ivy-Ochs, S., Kerschner, H., Kubik, P. W. & Schlüchter, C. Glacier response in the European Alps to Heinrich Event 1 cooling: the Gschnitz stadial. J Quaternary Sci **21**, 115-130, doi:10.1002/jqs.955 (2006).

19 Heinrich, H. Origin and Consequences of Cyclic Ice Rafting in the Northeast Atlantic Ocean During the Past 130,000 Years. Quaternary Res **29**, 142-152, doi:10.1016/0033-5894(88)90057-9 (1988).

20 Schmidt, R., Weckstrom, K., Lauterbach, S., Tessadri, R. & Huber, K. North Atlantic climate impact on early late-glacial climate oscillations in the south-eastern Alps inferred from a multi-proxy lake sediment record. J Quaternary Sci **27**, 40-50, doi:10.1002/jqs.1505 (2012).

21 Dielforder, A. & Hetzel, R. The deglaciation history of the Simplon region (southern Swiss Alps) constrained by Be-10 exposure dating of ice-molded bedrock surfaces. Quaternary Sci Rev **84**, 26-38, doi:10.1016/j.quascirev.2013.11.008 (2014).

22 Hippe, K. et al. Chronology of Lateglacial ice flow reorganization and deglaciation in the Gotthard Pass area, Central Swiss Alps, based on cosmogenic Be-10 and in situ C-14. Quat Geochronol **19**, 14-26, doi:10.1016/j.quageo.2013.03.003 (2014).

23 Wirsig, C., Zasadni, J., Christl, M., Akcar, N. & Ivy-Ochs, S. Dating the onset of LGM ice surface lowering in the High Alps. Quaternary Sci Rev **143**, 37-50 (2016).

24 Kelly, M. A., Ivy-Ochs, S., Kubik, P. W., von Blanckenburg, F. & Schluchter, C. Chronology of deglaciation based on Be-10 dates of glacial erosional features in the Grimsel Pass region, central Swiss Alps. Boreas **35**, 634-643 (2006).

25 Wölfler, A., Hampel, A., Dielforder, A., Hetzel, R. & Glotzbach, C. LGM ice extent and deglaciation history in the Gurktal and Lavantal Alps (eastern European Alps): first constraints from 10Be surface exposure dating of glacially polished quartz veins. J Quaternary Sci **Online Version of Record before inclusion in an issue**, doi:10.1002/jqs.3399 (2021).

26 Böhlert, R. et al. Application of a combination of dating techniques to reconstruct the Lateglacial and early Holocene landscape history of the Albula region (eastern Switzerland). Geomorphology **127**, 1-13 (2011).

27 Rolland, Y. et al. Deglaciation history at the Alpine-Mediterranean transition (Argentera-Mercantour, SW Alps) from Be-10 dating of moraines and glacially polished bedrock. Earth Surf Proc Land **45**, 393-410 (2020).

28 Maisch, M. Zur Gletscher- und Klimageschichte des alpinen Spätglazials. Geographica Helvetica **37**, 93-104, doi:10.5169/seals-58303 (1982).

29 Kerschner, H. in Klimawandel in Österreich: Die letzten 20.000 Jahre ... und ein Blick voraus Vol. 6 alpine space – man & environment (eds R. Schmidt, C. Matulla, & R. Psenner) 5-26 (Innsbruck University Press, 2009).

30 Federici, P. R. et al. Exposure age dating and Equilibrium Line Altitude reconstruction of an Egesen moraine in the Maritime Alps, Italy. Boreas **37**, 245-253, doi:10.1111/j.1502-3885.2007.00018.x (2008).

31 Kelly, M. A., Kubik, P. W., Von Blanckenburg, F. & Schlüchter, C. Surface exposure dating of the Great Aletsch Glacier Egesen moraine system, western Swiss Alps, using the cosmogenic nuclide Be-10. J Quaternary Sci **19**, 431-441, doi:10.1002/jqs.854 (2004).

32 Reitner, J. M., Ivy-Ochs, S., Drescher-Schneider, R., Hajdas, I. & Linner, M. Reconsidering the current stratigraphy of the Alpine Lateglacial: Implications of the sedimentary and morphological record of the Lienz area (Tyrol/Austria). E&G Quaternary Sci. J. **65**, 113-144, doi:10.3285/eg.65.2.02 (2016).

33 Heuberger, H. Die Alpengletscher im Spät- und Postglazial. Eiszeitalter und Gegenwart **19**, 270-275 (1968).

34 Lauterbach, S. et al. Environmental responses to Lateglacial climatic fluctuations recorded in the sediments of pre-Alpine Lake Mondsee (northeastern Alps). J Quaternary Sci **26**, 253-267 (2011).

35 Heiri, O. et al. Palaeoclimate records 60-8 ka in the Austrian and Swiss Alps and their forelands. Quaternary Sci Rev **106**, 186-205, doi:10.1016/j.quascirev.2014.05.021 (2014).

36 Rasmussen, S. O. et al. A stratigraphic framework for abrupt climatic changes during the Last Glacial period based on three synchronized Greenland ice-core records: refining and extending the INTIMATE event stratigraphy. Quaternary Sci Rev **106**, 14-28, doi:10.1016/j.quascirev.2014.09.007 (2014).

37 Li, H. Y., Spotl, C. & Cheng, H. A high-resolution speleothem proxy record of the Late Glacial in the European Alps: extending the NALPS19 record until the beginning of the Holocene. J Quaternary Sci **36**, 29-39 (2021).

38 Kruger, S. & Damrath, M. In search of the Bolling-Oscillation: a new high resolution pollen record from the locus classicus Lake Bolling, Denmark. Veg Hist Archaeobot **29**, 189-211 (2020).

39 Ammann, B. et al. Vegetation responses to rapid warming and to minor climatic fluctuations during the Late-Glacial Interstadial (GI-1) at Gerzensee (Switzerland). Palaeogeogr Palaeocl **391**, 40-59, doi:10.1016/j.palaeo.2012.07.010 (2013).

40 Brisset, E. et al. Lateglacial/Holocene environmental changes in the Mediterranean Alps inferred from lacustrine sediments. Quaternary Sci Rev **110**, 49-71 (2015).

41 Broecker, W. S. The Great Ocean Conveyor. Oceanography **4**, 79-89, doi:10.5670/oceanog.1991.07 (1991).

42 McManus, J. F., Francois, R., Gherardi, J. M., Keigwin, L. D. & Brown-Leger, S. Collapse and rapid resumption of Atlantic meridional circulation linked to deglacial climate changes. Nature **428**, 834-837, doi:10.1038/nature02494 (2004).

43 Thornalley, D. J. R., McCave, I. N. & Elderfield, H. Freshwater input and abrupt deglacial climate change in the North Atlantic. Paleoceanography **25**, PA1201, doi:10.1029/2009PA001772 (2010).

44 Bjorck, S., Rundgren, M., Ingolfsson, O. & Funder, S. The Preboreal oscillation around the Nordic Seas: terrestrial and lacustrine responses. J Quaternary Sci **12**, 455-465 (1997).

45 Hald, M. & Hagen, S. Early preboreal cooling in the Nordic seas region triggered by meltwater. Geology **26**, 615-618 (1998).

46 Young, N. E. et al. Deglaciation of the Greenland and Laurentide ice sheets interrupted by glacier advance during abrupt coolings. Quaternary Sci Rev **229**, 106091, doi:10.1016/j.quascirev.2019.106091 (2020).

47 Lambeck, K., Rouby, H., Purcell, A., Sun, Y. Y. & Sambridge, M. Sea level and global ice volumes from the Last Glacial Maximum to the Holocene. P Natl Acad Sci USA **111**, 15296-15303, doi:10.1073/pnas.1411762111 (2014).

48 Mitrovica, J. X., Gomez, N. & Clark, P. U. The Sea-Level Fingerprint of West Antarctic Collapse. Science **323**, 753-753, doi:10.1126/science.1166510 (2009).

49 Lin, Y. et al. A reconciled solution of Meltwater Pulse 1A sources using sea-level fingerprinting. Nat Commun **12**, 2015, doi:10.1038/s41467-021-21990-y (2021).

50 Ivanovic, R. F., Gregoire, L. J., Wickert, A. D., Valdes, P. J. & Burke, A. Collapse of the North American ice saddle 14,500 years ago caused widespread cooling and reduced ocean overturning circulation. Geophys Res Lett **44**, 383-392, doi:10.1002/2016gl071849 (2017).

51 Menviel, L., Timmermann, A., Timm, O. E. & Mouchet, A. Deconstructing the Last Glacial termination: the role of millennial and orbital-scale forcings. Quaternary Sci Rev **30**, 1155-1172, doi:10.1016/j.quascirev.2011.02.005 (2011).

52 Wittmeier, H. E. et al. Late Glacial mountain glacier culmination in Arctic Norway prior to the Younger Dryas. Quaternary Sci Rev **245**, doi:10.1016/j.quascirev.2020.106461 (2020).

53 Briner, J. P., Svendsen, J. I., Mangerud, J., Lohne, O. S. & Young, N. E. A Be-10 chronology of south-western Scandinavian Ice Sheet history during the Lateglacial period. J Quaternary Sci **29**, 370-380, doi:10.1002/jqs.2710 (2014).

54 Glasser, N. F. et al. Cosmogenic nuclide exposure ages for moraines in the Lago San Martin Valley, Argentina. Quaternary Res **75**, 636-646, doi:10.1016/j.yqres.2010.11.005 (2011).

55 Garcia, J. L. et al. Glacier expansion in southern Patagonia throughout the Antarctic cold reversal. Geology **40**, 859-862, doi:10.1130/G33164.1 (2012).

56 Moreno, P. I. et al. Renewed glacial activity during the Antarctic cold reversal and persistence of cold conditions until 11.5 ka in southwestern Patagonia. Geology **37**, 375-378, doi:10.1130/G25399a.1 (2009).

57 Sagredo, E. A. et al. Trans-pacific glacial response to the Antarctic Cold Reversal in the southern mid-latitudes. Quaternary Sci Rev **188**, 160-166, doi:10.1016/j.quascirev.2018.01.011 (2018).

58 Davies, B. J., Thorndycraft, V. R., Fabel, D. & Martin, J. R. V. Asynchronous glacier dynamics during the Antarctic Cold Reversal in central Patagonia. Quaternary Sci Rev **200**, 287-312, doi:10.1016/j.quascirev.2018.09.025 (2018).

59 Putnam, A. E. et al. Glacier advance in southern middle-latitudes during the Antarctic Cold Reversal. Nat Geosci **3**, 700-704, doi:10.1038/Ngeo962 (2010).

60 Putnam, A. E. et al. Warming and glacier recession in the Rakaia valley, Southern Alps of New Zealand, during Heinrich Stadial 1. Earth Planet Sc Lett **382**, 98-110, doi:10.1016/j.epsl.2013.09.005 (2013).

61 Lee, S. Y. et al. Late Quaternary glaciation in the Nun-Kun massif, northwestern India. Boreas **43**, 67-89, doi:10.1111/bor.12022 (2014).

62 Lemieux-Dudon, B. et al. Consistent dating for Antarctic and Greenland ice cores. Quaternary Sci Rev **29**, 8-20, doi:10.1016/j.quascirev.2009.11.010 (2010).

63 Hertl, A. Untersuchungen zur spätglazialen Gletscher- und Klimageschichte der Österreichischen Silvrettagruppe, Leopold-Franzens-Universität Innsbruck, (2001).

64 Alley, R. B. The Younger Dryas cold interval as viewed from central Greenland. Quaternary Sci Rev **19**, 213-226, doi:10.1016/S0277-3791(99)00062-1 (2000).

65 Briner, J. P. et al. Using in situ cosmogenic Be-10, C-14, and Al-26 to decipher the history of polythermal ice sheets on Baffin Island, Arctic Canada. Quat Geochronol **19**, 4-13, doi:10.1016/j.quageo.2012.11.005 (2014).

66 Buizert, C. et al. Greenland-Wide Seasonal Temperatures During the Last Deglaciation. Geophys Res Lett **45**, 1905-1914, doi:10.1002/2017gl075601 (2018).

67 Kaplan, M. R. et al. Glacier retreat in New Zealand during the Younger Dryas stadial. Nature **467**, 194-197, doi:10.1038/nature09313 (2010).

68 Cheng, H. et al. Timing and structure of the Younger Dryas event and its underlying climate dynamics. P Natl Acad Sci USA **117**, 23408-23417, doi:10.1073/pnas.2007869117 (2020).

69 Putnam, A. E. et al. Regional climate control of glaciers in New Zealand and Europe during the pre-industrial Holocene. Nat Geosci **5**, 627-630, doi:10.1038/NGEO1548 (2012).

70 Glasser, N. F., Harrison, S., Schnabel, C., Fabel, D. & Jansson, K. N. Younger Dryas and early Holocene age glacier advances in Patagonia. Quaternary Sci Rev **58**, 7-17, doi:10.1016/j.quascirev.2012.10.011 (2012).

71 Reynhout, S. A. et al. Holocene glacier fluctuations in Patagonia are modulated by summer insolation intensity and paced by Southern Annular Mode-like variability. Quaternary Sci Rev **220**, 178-187, doi:10.1016/j.quascirev.2019.05.029 (2019).

72 Saha, S., Owen, L. A., Orr, E. N. & Caffee, M. W. High-frequency Holocene glacier fluctuations in the Himalayan-Tibetan orogen. Quaternary Sci Rev **220**, 372-400, doi:10.1016/j.quascirev.2019.07.021 (2019).

73 Fischer, A., Seiser, B., Waldhuber, M. S., Mitterer, C. & Abermann, J. Tracing glacier changes in Austria from the Little Ice Age to the present using a lidar-based high-resolution glacier inventory in Austria. Cryosphere **9**, 753-766, doi:10.5194/tc-9-753-2015 (2015).

74 Land Tirol. (Land Tirol, Innsbruck, 2021).

75 swisstopo. (Bundesamt für Landestopografie, Wabern, 2021).

76 Hartl, L., Felbauer, L., Schwaizer, G. & Fischer, A. Small-scale spatial variability in bare-ice reflectance at Jamtalferner, Austria. Cryosphere **14**, 4063-4081 (2020).

77 Fischer, A., Fickert, T., Schweizer, G., Patzelt, G. & Gross, G. Vegetation dynamics in Alpine glacier forelands tackled from space. Sci Rep-Uk **9**, 13918, doi:10.1038/s41598-019-50273-2 (2019).

78 WGMS. Global Glacier Change Bulletin No. 4 (2018–2019). Global Glacier Change Bulletin, doi:doi:10.5904/wgms-fog-2021-05 (2021).

79 Lal, D. In situ-produced Cosmogenic Isotopes in Terrestrial Rocks. Annu Rev Earth Pl Sc **16**, 355-388, doi:10.1146/annurev.ea.16.050188.002035 (1988).

80 LDEO. Separation and Purifiation of Quartz from Whole Rock. 8 (2012).

81 LDEO. Extraction of Beryllium from Quartz. 19 (2012).

82 Nishiizumi, K. et al. Absolute calibration of Be-10 AMS standards. Nucl Instrum Meth B **258**, 403-413, doi:10.1016/j.nimb.2007.01.297 (2007).

83 Balco, G., Stone, J. O., Lifton, N. A. & Dunai, T. J. A complete and easily accessible means of calculating surface exposure ages or erosion rates from Be-10 and Al-26 measurements. Quat Geochronol **3**, 174-195, doi:10.1016/j.quageo.2007.12.001 (2008).

84 Claude, A. et al. The Chironico landslide (Valle Leventina, southern Swiss Alps): age and evolution. Swiss J Geosci **107**, 273-291, doi:10.1007/s00015-014-0170-z (2014).

85 Stone, J. O. Air pressure and cosmogenic isotope production. J Geophys Res-Sol Ea **105**, 23753-23759, doi:10.1029/2000jb900181 (2000).

86 Linsbauer, A. et al. The New Swiss Glacier Inventory SGI2016: From a Topographical to a Glaciological Dataset. Frontiers in Earth Science **9**, doi:10.3389/feart.2021.704189 (2021).

87 Moran, A. P., Kerschner, H. & Ivy-Ochs, S. Redating the moraines in the Kromer Valley (Silvretta Mountains) - New evidence for an early Holocene glacier advance. Holocene **26**, 655-664, doi:10.1177/0959683615612571 (2016).

88 Auer, I. et al. HISTALP - historical instrumental climatological surface time series of the Greater Alpine Region. Int J Climatol **27**, 17-46, doi:10.1002/joc.1377 (2007).

89 BMLRT. Vol. 2009-2018 (BMLRT, Vienna, 2021).

90 MacFarling Meure, C. et al. Law Dome CO2, CH4 and N2O ice core records extended to 2000 years BP. Geophys Res Lett **33**, L14810, doi:10.1029/2006GL026152 (2006).

91 NOAA Global Monitoring Laboratory. (NOAA Research, 2021).

92 Berger, A. & Loutre, M. F. in Supplement to: Berger, A; Loutre, M-F (1991): Insolation values for the climate of the last 10 million of years. Quaternary Science Reviews, 10(4), 297-317, https://doi.org/10.1016/0277-3791(91)90033-Q (PANGAEA, 1999).

Figures

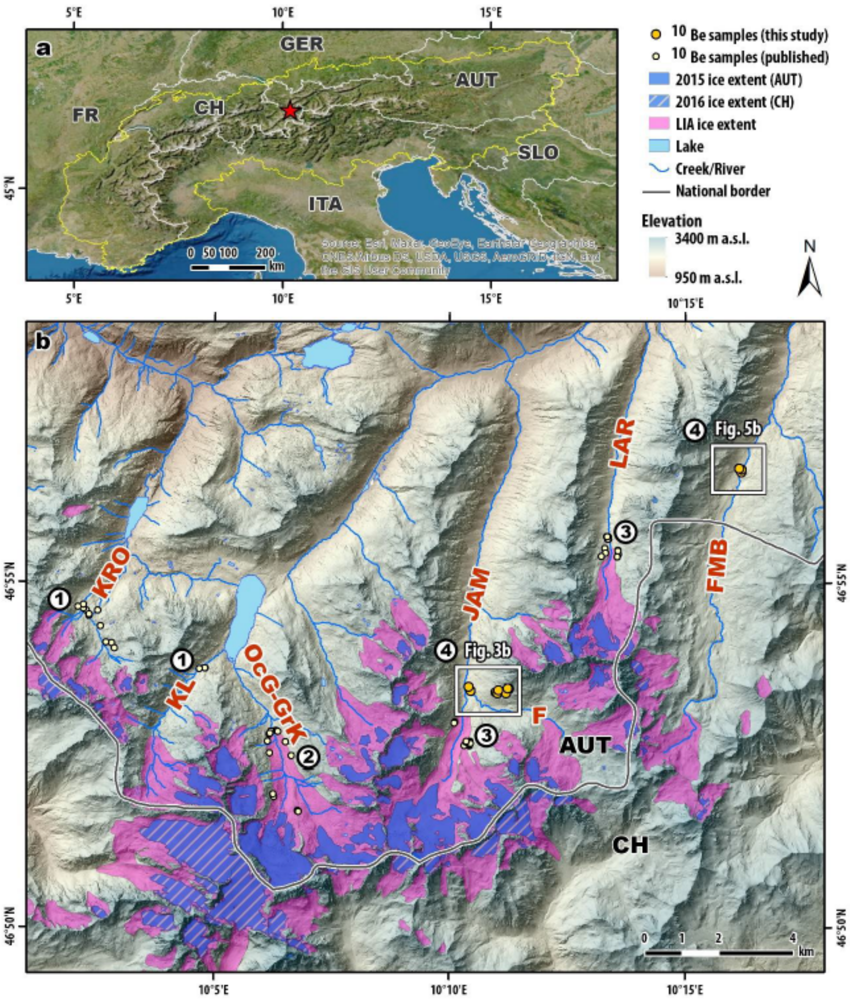

Figure 1

Location of study sites. **(a.)** Overview of the European Alps (yellow line); red star symbol marks Silvretta region, a glaciated area at the transition zone between the Western and the Eastern Alps. **(b.)** Investigated valleys in the north-facing part of the Silvretta region. Ice extents during the Little Ice Age (LIA) are depicted in pink, modern glacier extents indicated with blue signature (glacier extents of 2016 for Switzerland CH; glacier extents 2015 for Austria AUT) [73,86]. DEMs ©swisstopo, ©Land Tirol, and ©Land Vorarlberg. Valleys with previously published ^{10}Be moraine records from West to East: Kromertal (KRO) and Klostertal (KL) #1: Moran, et al. [87], Ochsental (OcG-GrK) #2: Braumann, et al. [17], Jamtal (JAM) with tributary valley Futschöltal (F) and Laraintal (LAR) #3: Braumann, et al. [9] and #4: this study, FMB – Fimbatal (#4: this study).

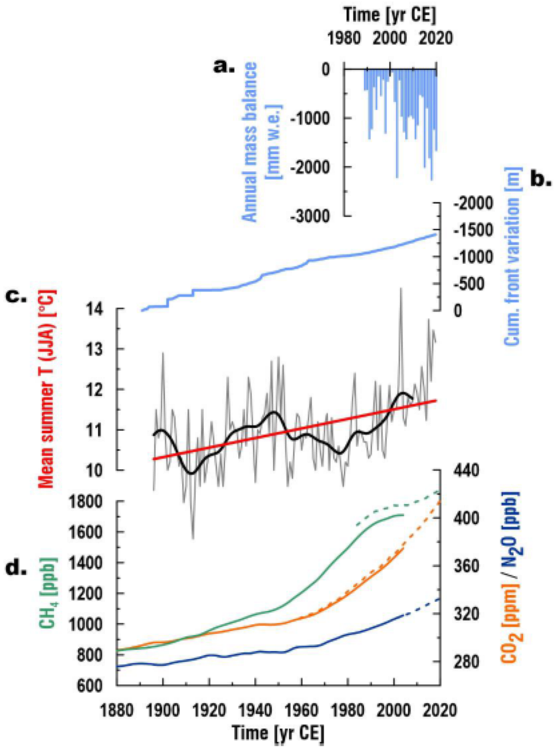

Figure 2

Response of Jamtal glacier to greenhouse gas emissions and rising temperatures over the past decades. **(a.)** Mass balance record of Jamtal glacier (1989-2020 CE) with negative values ranging between -62 mm water equivalent (w.e.) (2000 CE) and -2276 mm water equivalent (2018 CE) [78]. **(b.)** Front variation of Jamtal glacier (1891-2019) showing retreat of ca. 1.5 km since 1891 CE [78]. **(c.)** Mean summer temperature (grey line) at meteorological station Galtür (station number: 101949; 1587 m a.s.l.) overlain with 20 yrs low pass filter (black line) [88,89]. **(d.)** Mean annual atmospheric greenhouse gas concentrations (1880-2004) derived from Law Dome ice core (solid lines) [90]. Globally averaged marine surface annual data of CH_4 (1984-2020 CE; green dashed line), CO_2 (1959-2020; orange dashed line), and N_20 (2001-2020; blue dashed line) provided by [91].

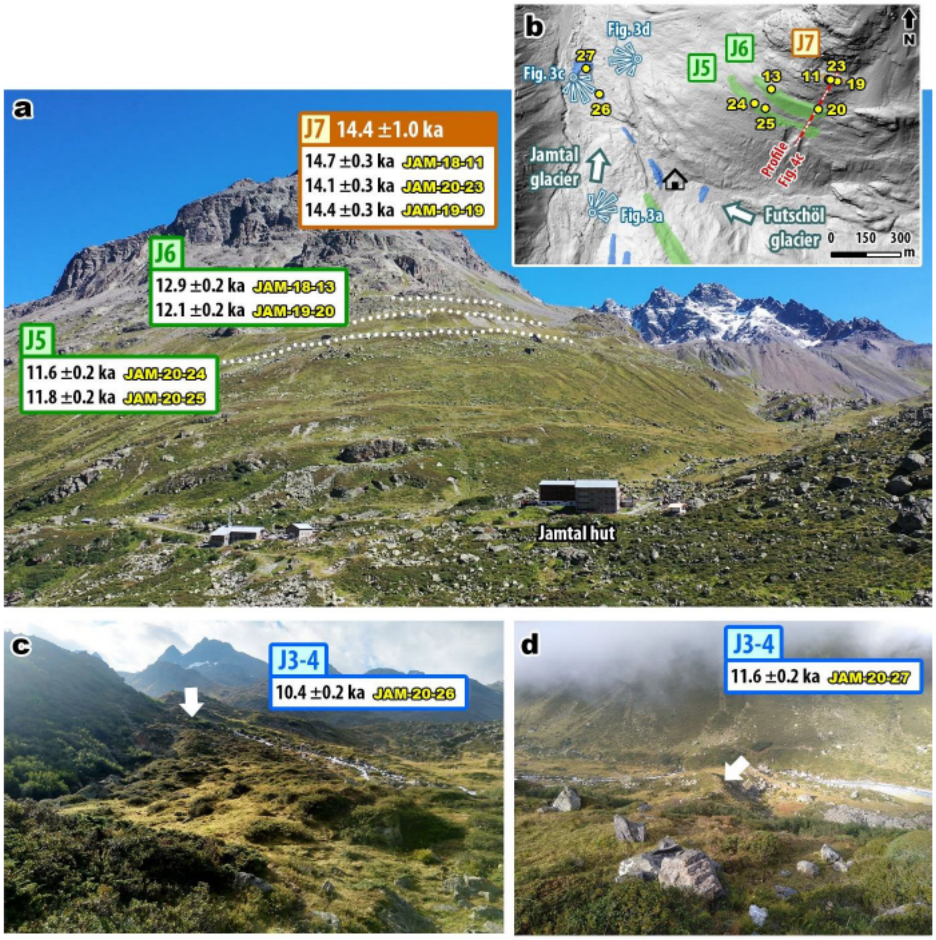

Figure 3

Photographs and map of sampled valley sections at Jamtal. **(a.)** Moraine sequence (dotted lines) evidence confluence of tributary (Futschöl) glacier with the main (Jamtal) glacier during the LG. The uppermost landform J7 indicates a stable ice margin position during (Pre-)Bølling times. J6 and J5 were deposited during the YD and suggest a lowering of the ice surface of ca. 55 m from the early YD to its end. For unedited photograph, we refer to Figure S2. **(b.)** Map showing sample and landform locations at Jamtal (DEM provided by © Land Tirol). **(c.)** Lateral moraine set deposited during the EH. The inner of two ridges (arrow) features boulder age JAM-20-26 and is (due to its position) several centuries younger compared to **(d.)** sample JAM-20-27 taken from the terminal section of J3-4. The statistically identical ages of J5 and JAM-20-27 suggest that the valley flank displayed in (a.) deglaciated within centuries during the YD-EH transition.

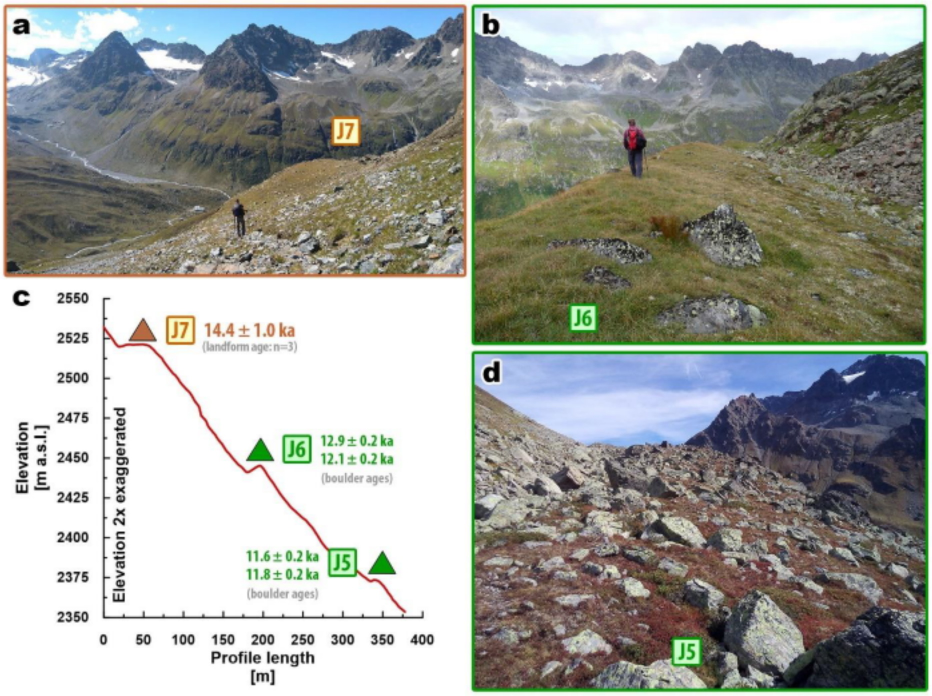

Figure 4

Closeups of dated moraines **(a.)** J7, **(b.)** J6 and **(d.)** J5 highlight different geomorphological characteristics of the three landforms. **(c.)** Profile along LG valley flank (for location see Figure 3b) indicating ice surface positions at different times during the LG.

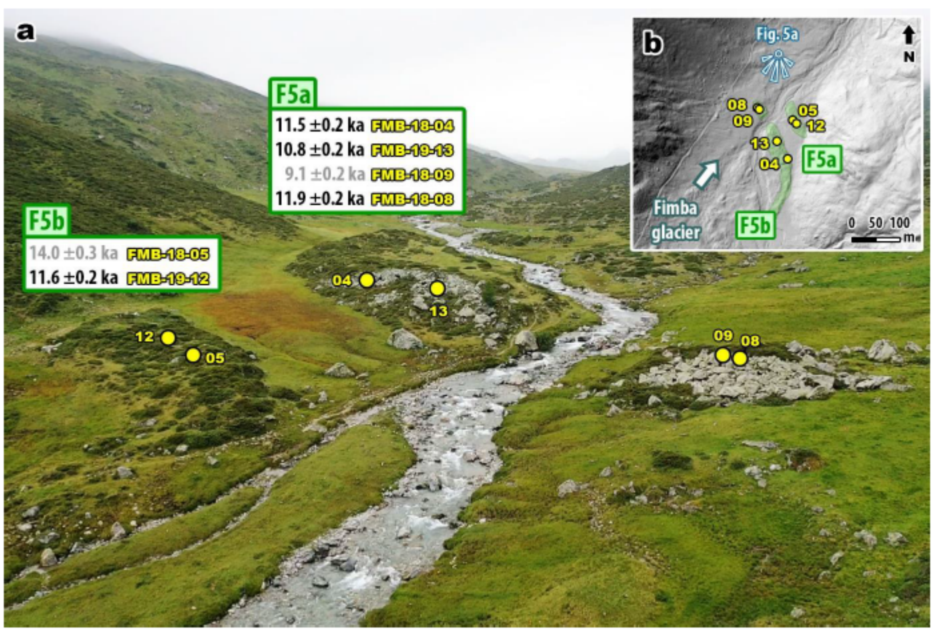

Figure 5

Photograph and map of sampled valley sections at Fimbatal. **(a.)** Photograph of F5a and F5b moraines indicating stable termini of Fimba glacier toward the end of the YD at an elevation of c. 2040 m a.s.l.; outliers are colored in gray. **(b.)** Map showing sample and landform locations at Jamtal (DEM provided by © Land Tirol).

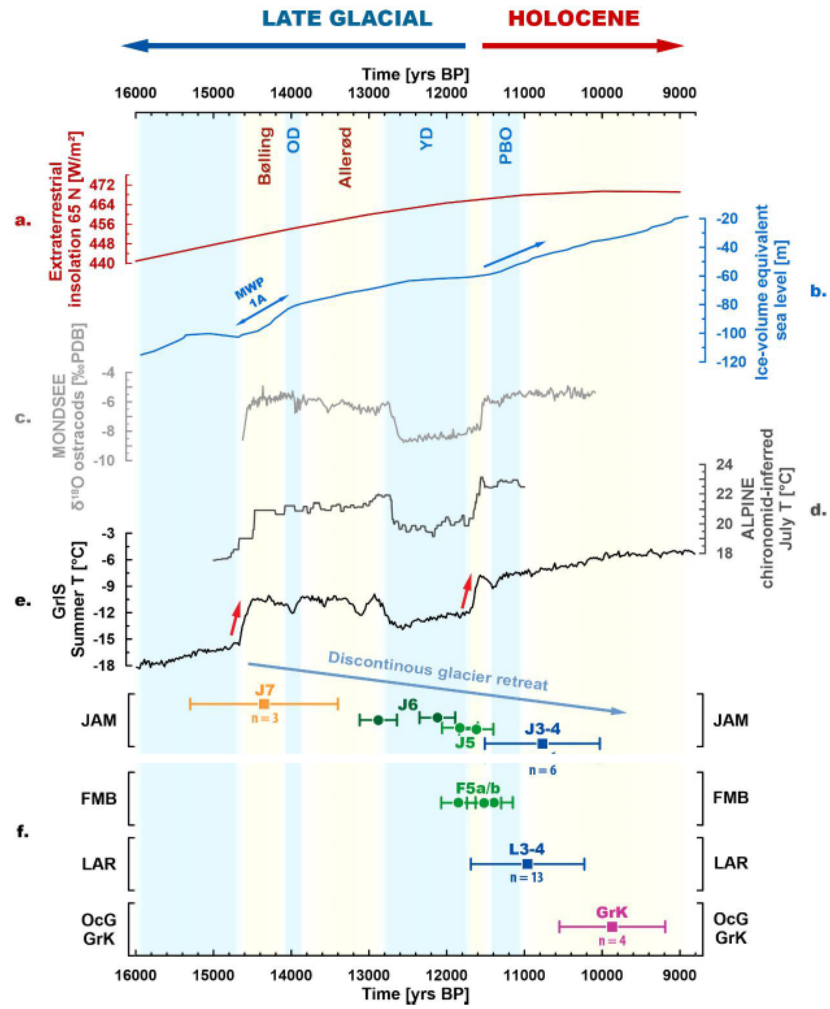

Figure 6

Silvretta mountain glacier records correlated with solar insolation, sea-level rise, and climate proxy records from different regions in the Northern Hemisphere. **(a.)** Insolation at 65N [92] gradually increases during the LG and is a natural forcing for climate warming during this period. **(b.)** Global sea-level rise due to deglaciation of the cryosphere [47]; note increased rate of change between 14.5 and 14 ka, and 11.4 ka onwards. **(c.)** Local high-resolution ostracod record from lake Mondsee [34]. **(d.)** Chironomid-inferred summer temperature stack record for the Alpine region [35]. **(e.)** Summer temperatures (as driving factor for mountain glacier oscillations) from Greenland Ice Sheet (GrIS) reconstructed based on oxygen isotopes in Greenland ice cores [66]. Temperatures reconstructed based on different methods and from different regions in the Northern Hemisphere agree well and capture the YD stadial as well as the two bracketing episodes of rapid climate warming, the Pre-Bølling to Bølling transition and the YD-EH transition. **(f.)** Glacier stabilization during general LG warming indicated by moraines deposited during Oldest Dryas to Bølling transition (J7), the YD (Egesen moraines J6, J5, and F5a/b), and the EH (J3-4 and L3-4) is this study and Braumann, et al. [9]. By 10 ka, Silvretta glaciers have retreated to positions that resemble (subsequent) LIA extents indicated by the ^{10}Be moraine record in the adjacent Ochsental [17]. Moraine ages ($n \geq 3$) are shown with rectangles, individual boulder ages with circles. Kernel plots of moraine ages are provided in the supplement (Figure S1). For the spatial context of the displayed ^{10}Be records, see Figure 1b and Figure 7.

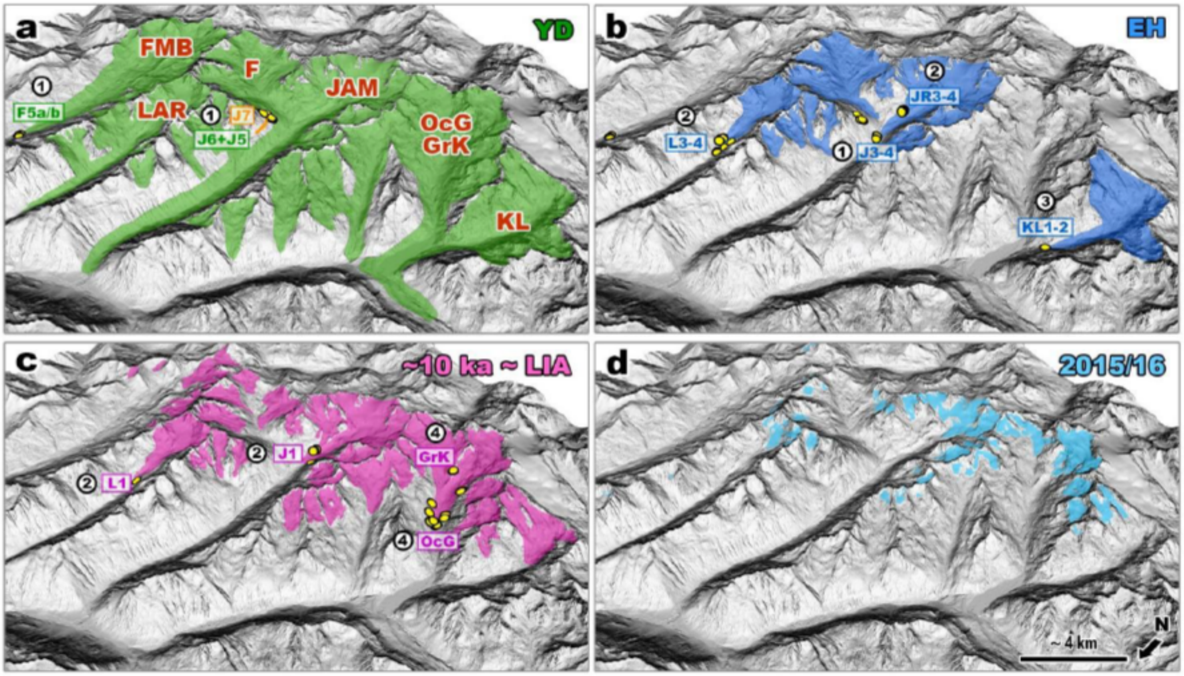

Figure 7

Possible extents of Silvretta glaciers during the **(a.)** the later YD, **(b.)** the EH, **(c.)** around 10 ka and during the LIA, and **(d.)** in 2015/16 CE. Positions of dated boulders are indicated with yellow symbols across all valleys and time slices and are published in this study (#1), in Braumann, et al. [9] (#2), in Moran, et al. [87] (#3), and in Braumann, et al. [17] (#4). IDs of corresponding moraines are adopted from original publications and are shown in rectangles. Ice margins positions with geochronological data available (yellow circles) are reliable. All other ice margins in (a.) and (b.) are estimates and are based on Hertl [63]. LIA and modern ice margins are taken from the Austrian and the Swiss glacier inventories, respectively [73,86]. The Jamtal moraine record in the context of previously published moraine records of the region indicates that the transition from YD to EH ice extents occurred within a few centuries.

Supplementary Files

This is a list of supplementary files associated with this preprint. Click to download.

- Braumannetal.SUPPLEMENTMorainesintheAustrianAlpsrecordrepeatedphasesofglacierstabilizationthroughtheLateGlacialandtheEarlyHolocene.pdf